A Self-Powered 50-Mb/s OOK Transmitter for Optoisolator LED Emulation

Sreenivasa Mallia S, Sreeram NS, Sudhir Komarla Adinarayana, and Sankaran Aniruddhan, *Senior Member, IEEE*

***Abstract*— Isolators are used to eliminate ground loops, and also to protect circuits that are sensitive to high voltages. Optoisolators are normally deployed for these purposes, but they suffer from several limitations, such as low speed of operation and temperature instability. In this paper, an ON–OFF keying (OOK) transmitter (TX) is designed so as to emulate and serve as an alternative to optoisolators, without significant changes to the rest of the system. The TX primarily consists of a voltage clamp circuit to convert input current into voltage, a discharge circuit to avoid metastability, and a 300–700-MHz spread-spectrum (SS) oscillator. The start-up and die-down times of the oscillator are optimized for maximum data speed. SS modulation of the oscillator output restricts radiative emissions to within permissible limits. The TX derives power from the input data (current) signal itself, thereby operating without any external power supply, and supports speeds of up to 50 Mb/s. The TX was fabricated in a BiCMOS semiconductor process and tested using an OOK receiver.**

***Index Terms*— Common mode transient immunity (CMTI), current to constant voltage converter, digital isolator, discharge circuit, frequency stability, ON–OFF keying (OOK), relaxation oscillator, reverse blocking circuit (RBC), spread-spectrum modulation (SSM), start-up circuit.**

I. INTRODUCTION

ISOLATORS are interface circuits that provide galvanic isolation between two communicating blocks. They ensure electrical insulation and isolation [1], [2], but at the same time, allow reliable data transmission between the two blocks. Fundamentally, they also help in eliminating ground loops and offer protection for high-voltage-sensitive circuits. Finally, they aid in isolating the desired signal from common mode noise and fast transients. In applications where common mode noise can be expected and human-electronics interactions are inevitable (e.g., a cardiograph), the isolators act as an interface ensuring safety and reliability. Finally, they are indispensable in several industrial applications that are susceptible to electrical surges, fast transients, and high noise floors.

Fig. 1 shows the block diagram of a generic isolation system. The sensor takes in information, which is processed by the signal conditioning block, which then controls the high-voltage portion of the system. The systems have some circuits working at low voltage (e.g., battery) and some circuits working from high voltage (e.g., power supply). Thus, in case of direct connection, any high-voltage transients in the power supply can damage the low voltage circuits or can cause harm to the user of the system. In such a case, the isolator is used as a level shifter and for safety purposes. Any common mode noise is dropped across the isolator, thus preventing the damage of high-voltage-sensitive circuits. Common mode transient immunity (CMTI) represents the tolerable rate of the change of common mode voltage so as to not affect the output of the device.

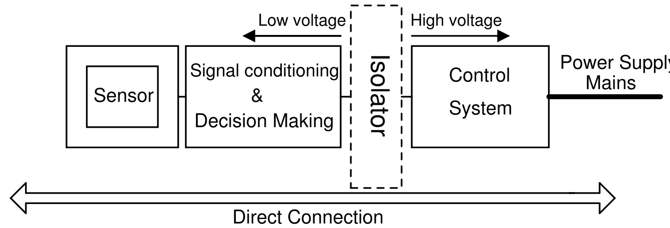

Fig. 1. Example of a system that uses an isolator.

The isolation barrier can be considered as the core of an isolator. Depending on the medium used as the isolation barrier and the physical quantity used to transfer data across it, the isolators are principally classified as optoisolators, capacitive isolators, and inductive isolators [3], as shown in Fig. 2. In optoisolators, the isolation barrier is the interspace between the transmitter (TX) and the receiver (RX), and the light is used to transfer data across the barrier. Capacitive isolators use a capacitor in between the TX and RX, and the interspace between the plates of the capacitor acts as the isolation barrier. Change in electric field is used to transfer data signal across isolation barrier [2]. A transformer is used in the inductive isolators for isolation, and the gap between primary and secondary windings acts as the isolation barrier. Change in magnetic field is used to transfer data across the barrier [4].

Optoisolators (often implemented in GaAs technology) are deployed in many systems due to their low cost and ease of fabrication. They do not cause and are not susceptible to radiative emissions, making them a popular choice for industrial applications. However, they suffer from several limitations, such as low speed of operation (<50 Mb/s) [3], [5] and temperature instability. Moreover, LED performance degrades with time [6], and the multichannel devices are hard to fabricate because of cross talk issues. Finally, optoisolators have much smaller CMTI (<35 KV/μs) when compared with other types of isolators. With recent developments in

Manuscript received May 24, 2016; revised September 22, 2016 and November 25, 2016; accepted November 26, 2016. Date of publication February 13, 2017; date of current version March 3, 2017. This paper was approved by Associate Editor Ali M. Niknejad.

S. Mallia S and S. Aniruddhan are with the Department of Electrical Engineering, IIT Madras, Chennai, India (e-mail: ee12s039@ee.iitm.ac.in; ani@ee.iitm.ac.in).

Sreeram NS and S. K. Adinarayana are with Texas Instruments (India) Pvt. Ltd., Bengaluru, India (e-mail: nssreeram@ti.com; sudhir_komarla@ti.com).

Color versions of one or more of the figures in this paper are available online at http://ieeexplore.ieee.org.

Digital Object Identifier 10.1109/JSSC.2016.2633577

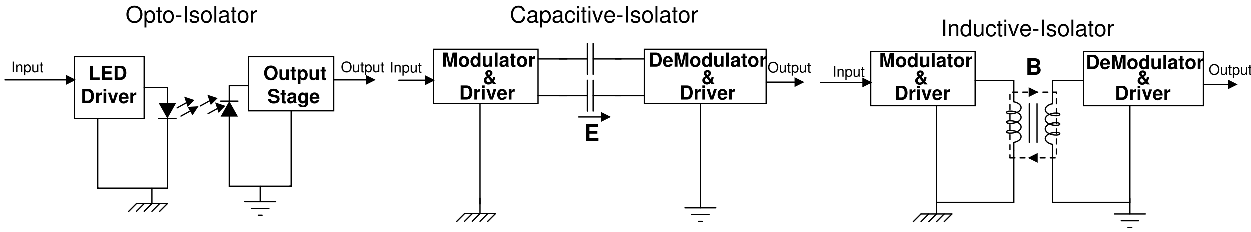

Fig. 2. Classification of isolators.

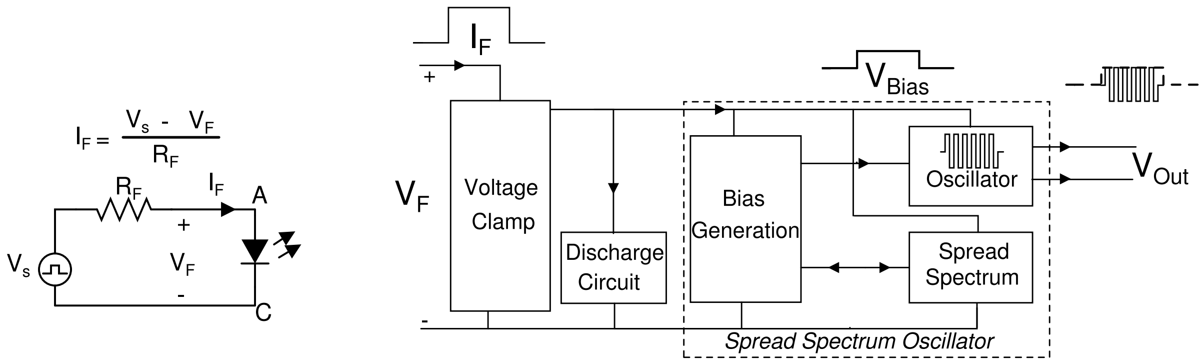

(a) (b)

Fig. 3. LED TX and block diagram of proposed TX. (a) LED TX with input data source. (b) Block diagram of TX.

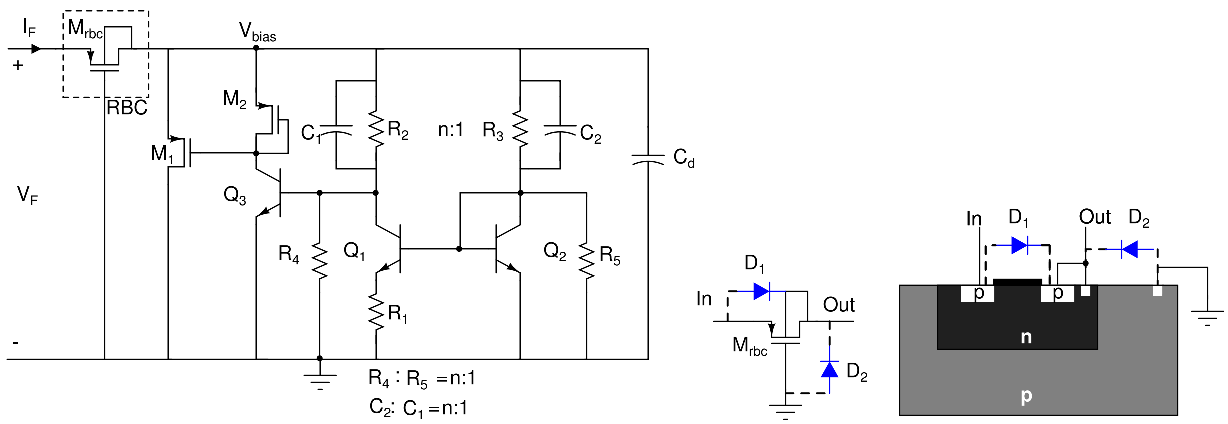

(a) (b)

Fig. 4. (a) Voltage clamp circuit. (b) RBC.

CMOS technology, CMOS digital isolators have emerged as competitors to optoisolators, exhibiting high speed and better reliability. This paper presents the design and implementation of an OOK TX based on capacitive isolation. The aim of this paper is to develop and present an isolation scheme that can be used as drop-in replacement for a conventional optoisolator, without significant changes to the rest of the system.

II. Optoisolator Transmitter Model

ON–OFF keying (OOK) is inherently implemented in the optoisolators by the LED, which acts as a TX. The LED is a transducer that converts electric signals into light signals, and derives its power from the input data signal (current). It eliminates the need for an external power supply, unlike conventional digital isolators. The TX in this paper was modeled to replace an LED while presenting the same electrical characteristics [7]. The block diagram of the TX is shown in Fig. 3(b). The TX detects the presence of the data signal [8] by input current in the range 3–8 mA, based on the configuration shown in Fig. 3(a). This current is used to generate a supply voltage using a voltage clamp circuit and power all other circuit blocks—oscillator, spread-spectrum (SS) modulator, and bias generator. The TX transmits an electrical wave (analogous to the light wave in the LED) across the isolation barrier in the presence of data. The voltage clamp ensures unidirectional operation of the block so as to electrically emulate the LED. For better transient performance, it has to be ensured that all critical nodes in the TX quickly settle to zero voltage

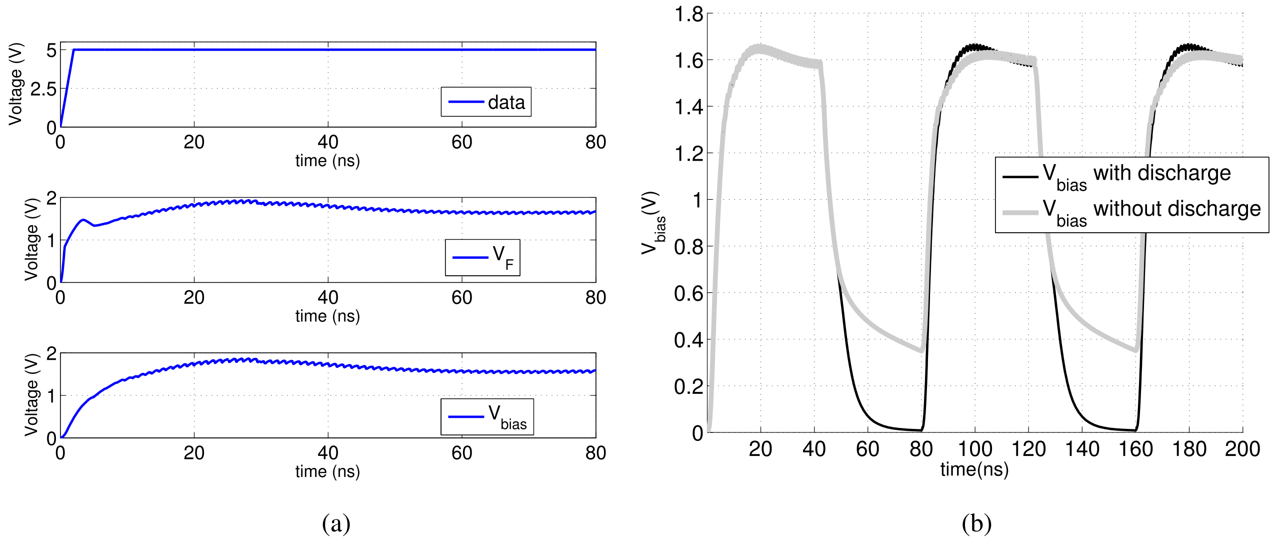

Fig. 5. (a) Settling behavior of V_{clamp}. (b) V_{bias} node with and without discharge circuit.

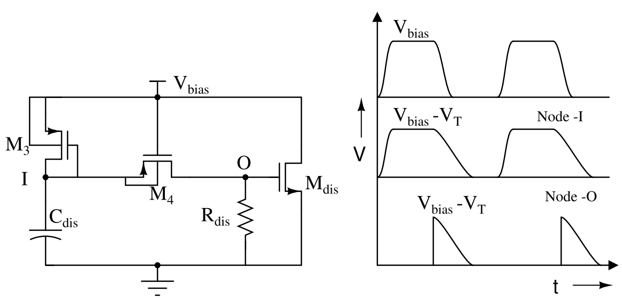

Fig. 6. Discharge circuit and its operation.

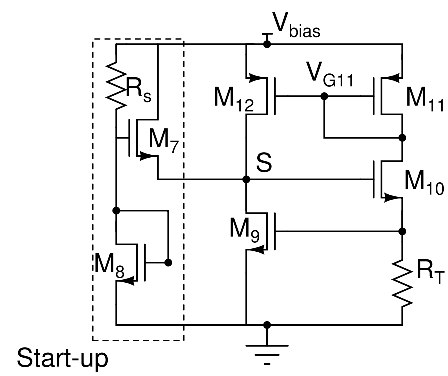

Fig. 8. (V_T/R_T) current generation circuit.

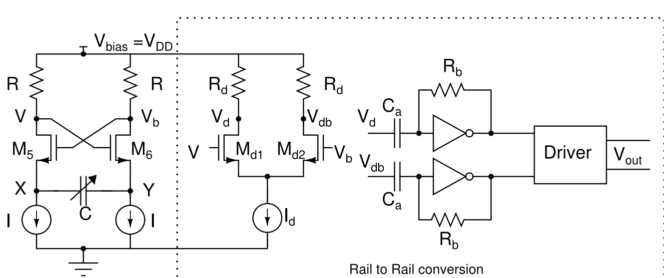

Fig. 7. Relaxation oscillator and output rail-to-rail conversion.

in the absence of a data signal, and this is ensured by the discharge circuit. The OOK is implemented in the system through a differential oscillator, which has good common mode rejection. SS modulation (SSM) is implemented in the oscillator to restrict radiative emissions to be within permissible limits and thereby meet regulatory standards [9], [10]. The bias generation circuits produce the desired operating currents for the oscillator and other subsystems. Finally, the TX also includes circuits to improve the start-up of the different blocks, which are not explicitly shown in Fig. 3(b).

III. System Implementation

A. Voltage Clamp Circuit

Good temperature stability of output voltage, low reverse current, and fast settling is the important design considerations for the voltage clamp circuit. A diode clamp cannot be used due to the large change in forward voltage (V_F) with temperature and process variations. A reference circuit based on the gate-source voltage of an MOS device is an alternative choice. However, it has temperature, process, and input current dependencies that cannot be easily avoided. Therefore, the clamp circuit shown in Fig. 4(a) is proposed, so as to ensure that V_F is largely independent of temperature and process variations. This circuit is similar to a bandgap circuit [11], but with the output voltage being a scaled version of the bandgap voltage.

The operation of the clamp circuit is as follows. Initially, input current starts flowing in Q_2, R_2, R_3, R_5, and R_4. This causes Q_1 to turn on, as Q_2 and Q_1 form a current mirror pair. Once enough voltage develops across R_4, Q_3 turns on. The circuit then operates in negative feedback, ensuring that the voltage at the collector of Q_1 is the same as that of Q_2, i.e., V_{BE}. Resistors R_2 and R_3 are in the ratio n:1, leading to

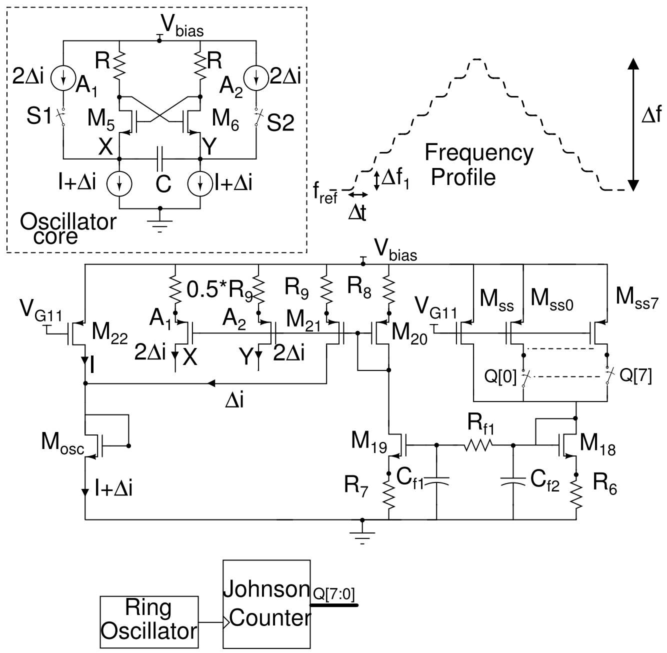

Fig. 9. SSM implementation.

a 1:n ratio of currents. Any extra input current is drained by M1 and M2. The clamp voltage V_{bias} is set by the feedback loop to be equal to

$$V_{\text{bias}} = V_{\text{BE}} + R_2 \cdot \left(\frac{V_{\text{BE}}}{R_4} + \frac{V_T \ln(n)}{R_1}\right). \quad (1)$$

Values of R_1, R_2, R_4, and n are set to obtain a temperature coefficient less than 0.45 mv/°C. Since currents flowing in Q_2 and Q_3 are not equal, their base–emitter voltages are different. This error is not constant and varies with input current, process, and temperature, and V_{bias} is thus not a constant voltage. Over the input current range of 3–8 mA and across PVT variations, V_{bias} lies between 1.41 and 1.9 V. Capacitors C_1 and C_2 are used to improve the transient performance of the voltage clamp by providing a feed-forward path. The simulated transient settling behavior of this circuit is shown in Fig. 5(a).

The parasitic diodes of the bipolar transistors conduct in reverse direction, burning power unnecessarily. Therefore, it is important to ensure unidirectional operation of the TX. Use of a diode at the input limits V_{bias} and hence oscillator output swing. A reverse blocking circuit (RBC) is created by employing a pMOS transistor M_{rbc}, as shown in Fig. 4(b). M_{rbc} is turned on in the forward direction and conducts current with a voltage drop across it. In the reverse direction, M_{rbc} is OFF and its parasitic diodes block reverse current from flowing in the other transistors. Any applied reverse voltage is dropped across the parasitic diode D_1. The voltage drop across the RBC in the forward operation is ensured to be less than 100 mV over the input current range of 3–8 mA and PVT variations.

V_{bias} is the supply voltage for all circuits in the TX, and switching currents are drawn from this node. Therefore, a capacitor C_d is placed to reduce ripple, which introduces a circuit speed limitation. At higher data rates, this node takes a long time to discharge because of C_d, worsening the transient performance of the block.

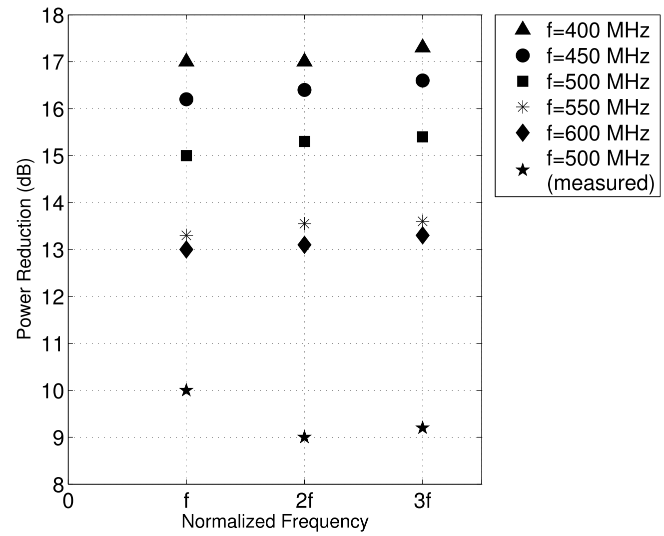

Fig. 10. Peak power reduction at different frequencies (simulated and measured).

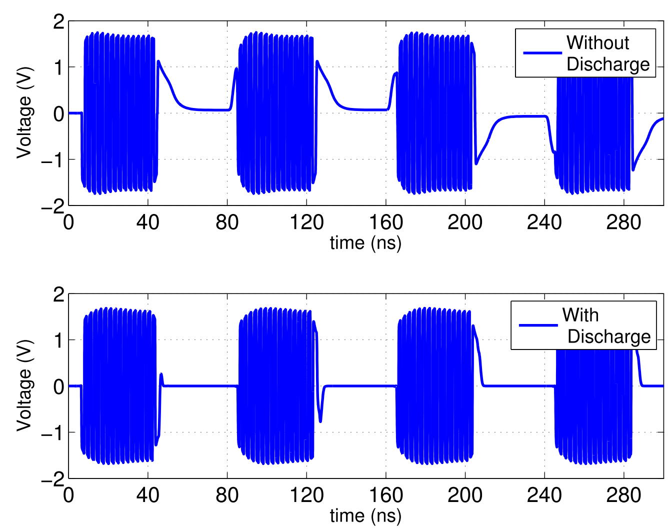

Fig. 11. Oscillator behavior with and without discharge circuit (simulation).

B. Discharge Circuit

Since there is no external power supply, the circuit blocks of the TX could potentially wake up with different initial conditions. This degrades the transient performance of the TX as different settling times are required each time a data-high signal is required to be transmitted. A dedicated discharge circuit, shown in Fig. 6, forces critical circuit nodes to ground and ensures that there is no circuit stuck in a metastable state when turned off. During the rising edge of V_{bias}, M_3 and M_4 are ON and OFF, respectively, while capacitor C_{dis} at Node-I charges to $V_{\text{bias}} - V_{\text{TP}}$, where V_{TP} is the threshold voltage of pMOS transistors. As the supply voltage rises above this value, both M_3 and M_4 turn off. During the falling edge of V_{bias}, M_4 turns on as the voltage at its gate decreases below the earlier value of $V_{\text{bias}} - V_{\text{TP}}$, and the capacitor C_{dis} discharges through M_4 and R_{dis}. M_{dis} turns on and discharges the V_{bias} node to ground at a rate that depends on its ON-resistance and the

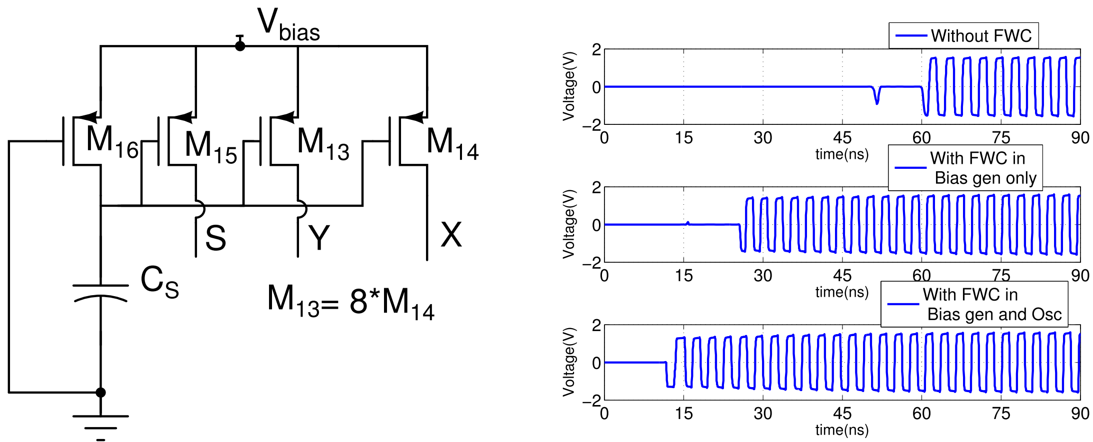

(a) (b)

Fig. 12. (a) FWC. (b) Oscillator start-up time comparison (simulation).

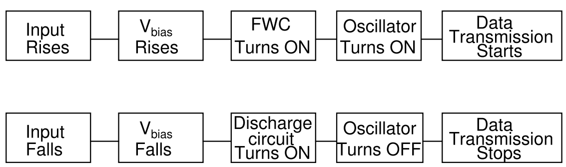

Fig. 13. Sequence of operation of different blocks when input changes.

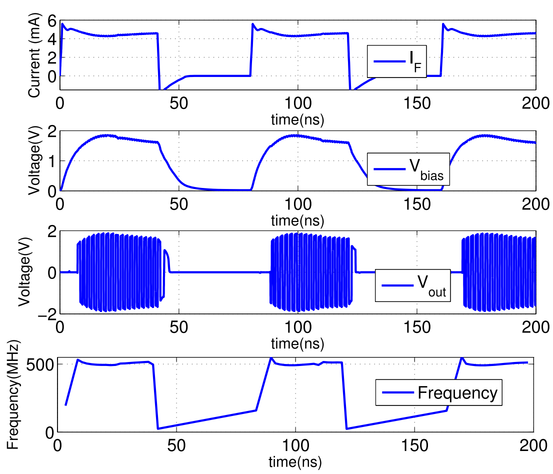

Fig. 14. Signals at various nodes during data transmission at 25 Mb/s (simulation).

total effective capacitance at the V_{bias} node. The voltage at Node-O drops at a rate decided by the value of R_{dis} and C_{dis}, which is chosen such that the voltage at Node-O is less than the threshold voltage of M_{dis} within the smallest bit period of operation. This ensures that M_{dis} is OFF during the next data high signal. Similarly, M_{dis} should be large enough such that it is able to discharge the V_{bias} node well within the smallest bit period. Dimensions of M_4 should be chosen, such that the voltage that drops across it is small when it is ON. Fig. 5(b) shows the simulated behavior of the V_{bias} node with and without the discharge circuit. Significant improvement in transient performance of the voltage clamp is observed, especially at high speeds.

C. Spread-Spectrum Oscillator

The oscillator forms the core of the OOK modulation scheme. Its start-up time and oscillation frequency variation across PVT are major design considerations. An *LC* oscillator has a fairly predictable frequency of oscillation as well as low supply dependence. However, the spiral inductor occupies significant die area, causing prohibitive increase in cost. As a replacement solution to an optoisolator that uses a compact LED device, the *LC* oscillator would be highly noncompetitive. A conventional ring oscillator, though easy to design, is not chosen because of its strong supply dependence. Its variant, the current starved ring oscillator, is another convenient choice, which is simple and also offers rail-to-rail swings. However, the necessity of a PVT-independent current source limits its start-up time and thereby the overall speed of the system. A CMOS source-coupled relaxation oscillator [12], [13], shown in Fig. 7, is chosen in this paper. The two current sources of value I charge and discharge the capacitor C in each oscillation period. The voltage across the capacitor varies between V_T and $-V_T$ in a triangular fashion, where V_T is the threshold voltage of MOS transistors M_5 and M_6. The frequency of oscillation f is given by

$$f = \frac{I}{2CV_T}. \tag{2}$$

Variation of V_T across process and temperature (>20%) is directly reflected in the frequency variation. To tackle this, a self-biased (V_T/R_T) current source (Fig. 8) is used to bias the oscillator.

A separate start-up circuit ensures that the oscillator does not remain in a zero current state [14]. The output drive strength of the TX is improved by ensuring rail-to-rail swing for the oscillator. As shown in Fig. 7, the oscillator core is followed by a differential amplifier, which acts as a buffer and isolates the oscillator core from other stages. Further gain and rail-to-rail operation are achieved using a pair of self-biased inverters. Finally, a driver stage is used to drive the isolation barrier.

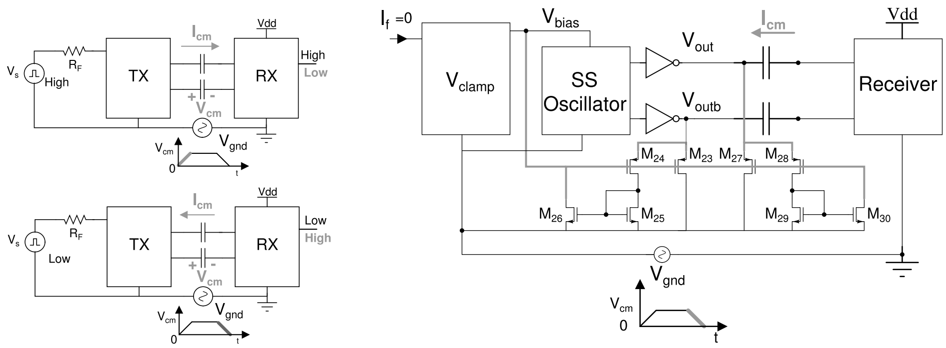

(a) (b)

Fig. 15. (a) CMTI false turn on and false turn off. (b) CMTI improvement circuit.

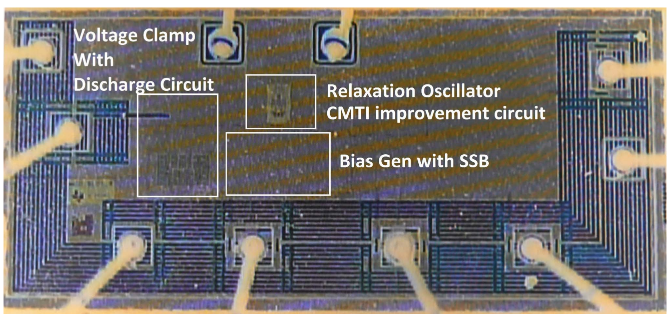

Fig. 16. Silicon die photograph of TX.

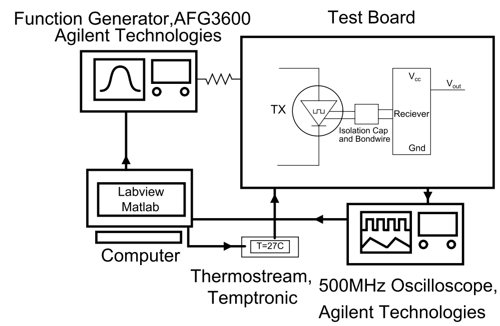

Fig. 17. Test setup for characterization of the TX.

Since the source-coupled relaxation oscillator described above is a current controlled oscillator, adding an SS current Δi to the bias current I should vary frequency by $\Delta f = ((\Delta i)/(2CV_T))$. However, due to the nonlinear effects in MOS transistors M_5 and M_6, an increase in their current leads to an increase in gate-source voltage $V_{\rm GS}$. Hence, the frequency spread is less than the expected value. The proposed solution to this issue is to use two additional current sources of value $2\Delta i$ to maintain a constant current in the transistors, as shown in Fig. 9.

The operation of the circuit is as follows. Switches S_1 and S_2 are controlled using the rail-to-rail complementary outputs of the oscillator. S_1 is turned on when transistor M_5 is ON. In this state, the currents flowing in M_5 and S_1 are $2I$ and $2\Delta i$, respectively. In the complementary state, S_2 turns on and ensures a current of $2I$ through M_6. A constant current $2I$, therefore, flows in the cross-coupled structure. At the same time, the charging and discharging current of the capacitor C is $I + \Delta i$, due to which the oscillation frequency changes.

A triangular frequency profile [15], [16] is preferred in the current system taking into account peak power reduction and speed constraints. A stepped-triangle profile can overcome speed limitations related to an ideal triangular profile, with minimal impact on SSM efficiency. In this paper, a low-pass-filtered version of the stepped-triangle profile was chosen so that the oscillator frequency traces a larger number of points. This achieves a spectrum that is closer to that of the ideal triangular profile, thus gaining better peak power reduction. A major goal of this paper was to minimize radioactive emissions. The output power level showed a relative lowering of around 15 dB compared with the case without SSM, in simulation. The circuit used to implement this SSM profile consisted of a ring oscillator running at a modulation rate of approximately 100 kHz, an 8-b Johnson counter to generate eight states (Q[7:0]), and current sources in parallel to generate Δi. Current sources $M_{\rm SS0} - M_{\rm SS7}$ are turned on and off through the series switches controlled by the Johnson counter. The bias voltage V_{G11} is generated from the circuit shown in Fig. 8. R_{f1}, C_{f1}, and C_{f2} act as a filter to generate a current with low-pass-filtered stepped-triangle profile. $M_{\rm osc}$ carries a current of $I+\Delta i$, and is used to set the operating point of the cross-coupled transistors for a bias current of I. The SS current of $2\Delta i$ is provided by M_{10}. The oscillator in this paper is designed to operate between 300–700 MHz, with a view to reducing the second-harmonic emissions in the 900-MHz cellular bands. This operating frequency range can be easily tuned for other applications by changing the capacitor C in the relaxation oscillator core. The oscillator achieves an *untrimmed* operating frequency deviation of $\pm 17\%$ around the center frequency across PVT variations (including SSM), which is better than that associated with conventional ring oscillators (around $\pm 25\%$). Fig. 10 shows the comparison of the peak power reduction achieved at different frequencies. As frequency increases, ON–OFF delay of switches S_1 and S_2 becomes significant, and the effectiveness of SSM improvement circuit reduces. The discharge circuit is used inside the oscillator too, to ensure that Node-X and Node-Y (Fig. 7) are discharged to zero when the data input

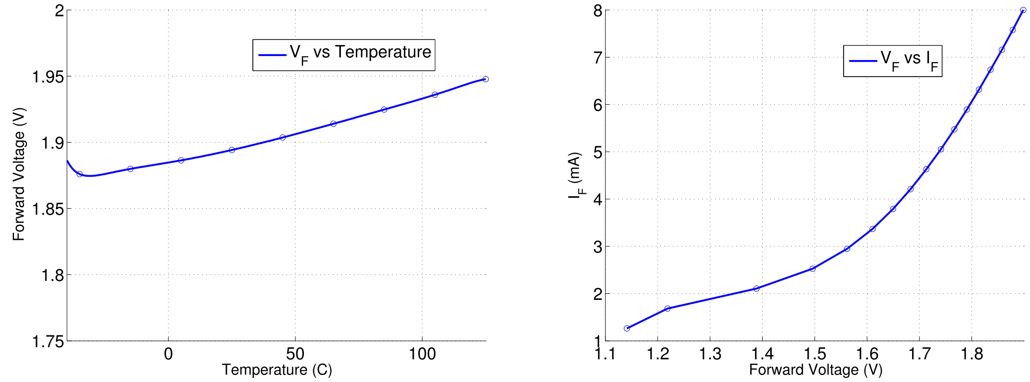

(a) (b)

Fig. 18. V_F characteristics. (a) V_F versus temperature. (b) V_F versus I_F.

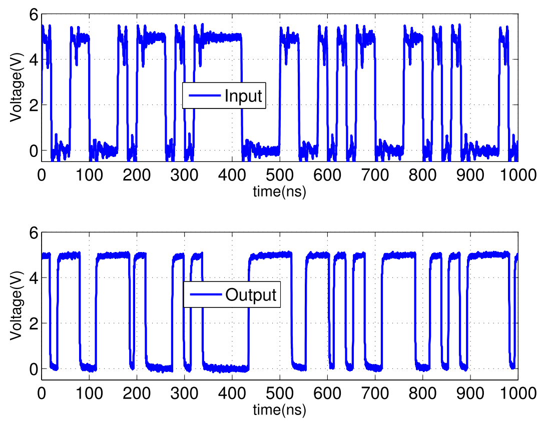

Fig. 19. Data transmission at 50-Mb/s PRBS.

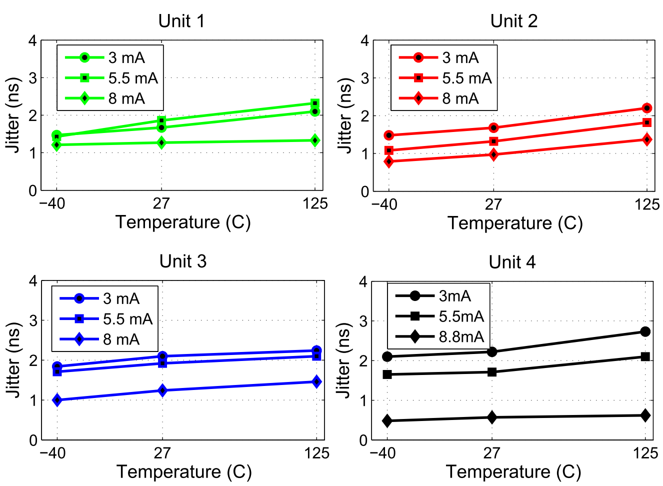

Fig. 20. Jitter (rise) characterization.

goes low. This improves the transient power down behavior of the oscillator. Fig. 11 shows the comparison of oscillator transient behavior with and without the discharge circuit.

D. Fast Wake-Up Circuit

A wakeup circuit is implemented, as shown in Fig. 12(a), to ensure fast start-up of the oscillator, thereby improving the transient response of the system. As V_{bias} rises, transistors M_{13}–M_{16} are ON, and the capacitor C_S is charged. Transistor M_{15} injects some current into Node-S of the current generation circuit of Fig. 8. At the same time, transistors M_{13} and M_{14} introduce intentional current mismatch (8 times) in the oscillator core (Fig. 7), due to which oscillation start-up is accelerated. Once the capacitor C_S charges to V_{bias}, transistors M_{12}–M_{15} turn off and the fast wake-up circuit (FWC) is idle. The sequence of operation of different blocks when input changes is shown in Fig. 13. A simulated comparison of oscillator start-up with and without the FWC is shown in Fig. 12(b). Fig. 14 shows the signals at different nodes of the system at a data rate of 25 Mb/s and at oscillator midband frequency of 500 MHz.

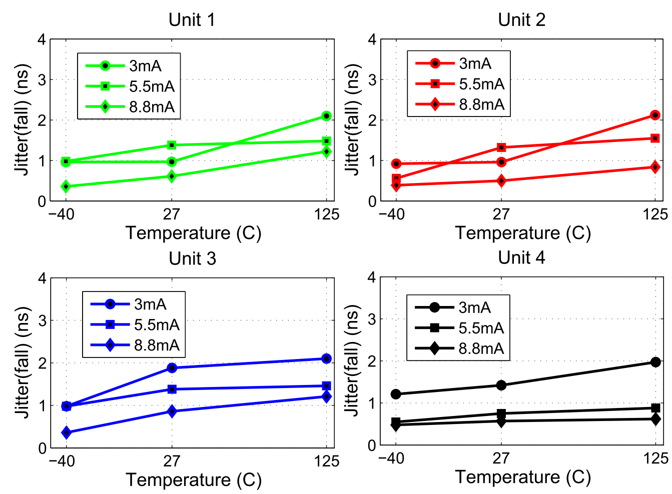

Fig. 21. Jitter (fall) characterization.

E. Common Mode Transient Immunity Improvement Circuit

CMTI is an important characteristic and metric of isolators. Common mode noise or ground noise is modeled by V_{gnd}, as shown in Fig. 15(a). During input data high and positive edge of V_{gnd}, a current I_{cm} is drawn from the circuit, and isolation capacitor charges to V_{cm}. Since the proposed TX in this paper is a current controlled block, increase in I_{cm} could result in the decrease of voltage V_{bias}. This could potentially cause a reduction in frequency of oscillation and result in the failure of signal detection by the RX. This event is termed a false turn off in optoisolators, because the LED turns off even when data input is high due to the lack of sufficient current. The present TX achieves a minimum CMTI of 75 KV/μs

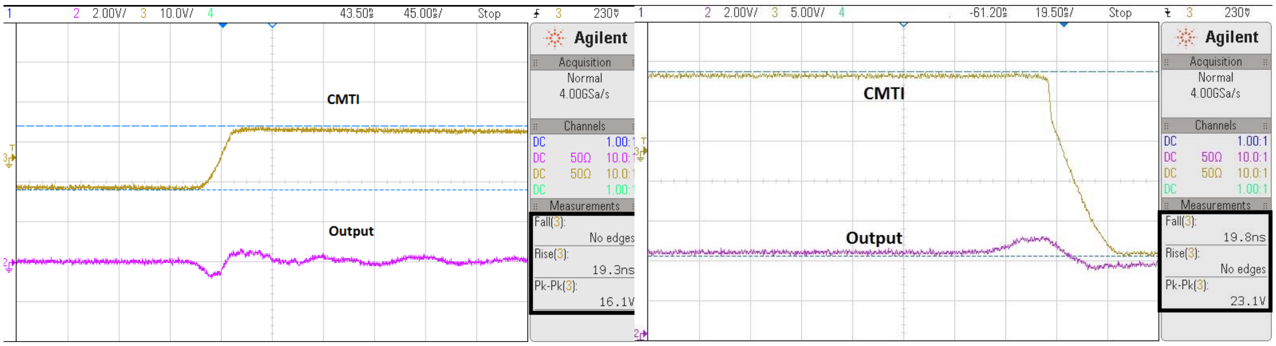

(a) (b)

Fig. 22. CMTI rise and fall event. (a) CMTI event at 75 KV/μs, data signal high. (b) CMTI event at 100 KV/μs, data signal low.

without false turn off by ensuring sufficient current margin at input and correct choice of C_d value. A similar case occurs when the data are low, where TX should ideally be OFF. However, during the negative edge of V_{gnd}, the isolation cap discharges from V_{cm} by pumping a current I_{cm} into the TX. The oscillator starts oscillating and RX falsely detects the presence of data. This causes a false turn on event in the optoisolators, where the LED turns on even when data input is low. The basic TX system exhibited a false turn on event for CMTI values less than 20 KV/μs, which was not considered to be sufficient. A CMTI improvement circuit is implemented to achieve larger CMTI compliance.

The basic idea behind the improvement circuit is to find an alternate path for I_{cm} to flow (other than the TX) during a CMTI event. An additional requirement is to ensure that this path is idle during normal operation. This is achieved by the circuit shown in Fig. 15(b). During a CMTI event, voltages at nodes V_{out} and V_{outb} increase. When these rise above V_T, transistors M_{23}, M_{24}, M_{27}, and M_{28} turn on as their gate voltage is connected to V_{bias} node whose value is 0 V. At nodes V_{out} and V_{outb}, current flow gets divided between the V_{bias} node and the CMTI improvement circuit. The current flowing into the V_{bias} node is again divided between different circuits (V_{clamp} and SS oscillator), and transistors M_{26} and M_{30} of the CMTI improvement circuit. These last two devices ensure that current flowing into the rest of the TX is negligible, and V_{bias} stays close to ground potential. Thus, false turn on is prevented in the TX, and a minimum CMTI of 100 KV/μs is observed in the simulation. This circuit is inactive during a CMTI ramp-up situation, because current is drawn from the clamp circuit and the voltage V_{bias} tries to decrease. Therefore, there is no possibility of a false turn on event.

IV. Experimental Results

The proposed TX was designed and fabricated in a Texas Instruments proprietary BiCMOS process. The TX occupies an active area of 0.13 mm^2 (Fig. 16), and was tested using an RX with a preamplifier and an envelope detector. Detailed testing was performed over a temperature range of −40 to 125 °C and an input current range of 3–8 mA, across four devices. The test setup used for the characterization of the TX chip is shown in Fig. 17. The capacitive isolation barrier and the associated

TABLE I
Test Results and Comparison With State of the Art

Characteristics	This work	[5]
Input Voltage (V_F, V)	1.75	4.5
Temperature Coefficient ($\frac{\Delta V_F}{\Delta T}$, $mv/$°C))	0.4	-
Reverse Current (I_R, nA)	20	-
Maximum Data rate ($Mbps$)	50	50
Propagation Delay, High-to-Low (t_{phl}, ns)	12.37	16
Propagation Delay, Low-to-High (t_{plh}, ns)	16.56	16
Pulse Width Distortion (PWD, ns)	6.57	1
Jitter (cycle-to-cycle, ns)	3	-
Minimum Common Mode Transient Immunity ($CMTI$, $KV/\mu s$)	75	10
Emissions Peak Power Reduction (P_C, dB)	10	-

details are proprietary information. Temperature stability is an important property for the optoisolators, where the temperature coefficient of the input voltage V_F is around −2 mV/°C. The proposed TX exhibits excellent V_F temperature stability, with an even smaller temperature coefficient of less than 0.4 mV/°C, as shown in Fig. 18(a). To further validate the similarity of V_F behavior between conventional optoisolators and the proposed TX, the input current I_F was plotted against the input voltage V_F, in Fig. 18(b). An exponential diode-like behavior can be observed in the expected operating current range of 3–8 mA. There were not enough corner parts to ensure that the V_F variation is low over process variations.

A PRBS data sequence exercises the limits of oscillator start-up and die-down transient behavior, because the rising and falling edges are unpredictable. Therefore, for full functional verification, a PRBS sequence was used for data transmission at 50 Mb/s, and the results are shown in Fig. 19 (note that the RX has inverted logic). A preexisting proprietary OOK RX was used to receive the signal and measure its quality in terms of cycle-to-cycle jitter, pulsewidth distortion (PWD), and overall data rate. Above 50 Mb/s, bit error rate (BER) increases beyond acceptable levels because of rise in jitter and PWD. If higher BER levels are tolerable, the TX can be operated beyond 50 Mb/s. Variation of jitter across different units, temperature, and input current is shown in Figs. 20 and 21. CMTI experiments were conducted to check for false turn

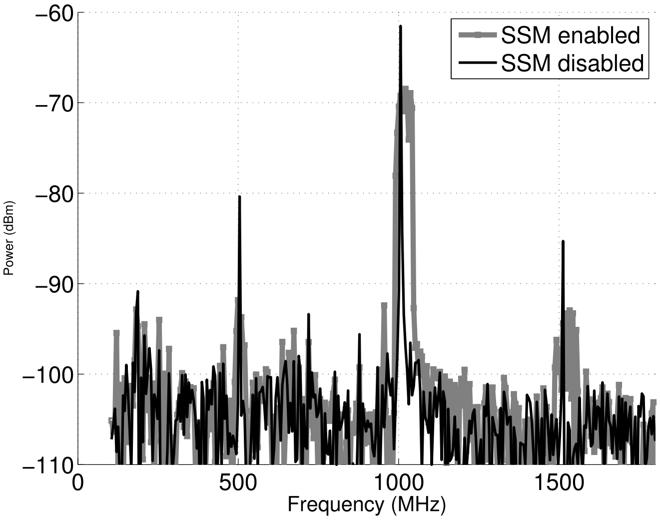

Fig. 23. Emissions results with and without SSM.

on/off, and the output transient waveforms for data high and low signals are shown in Fig. 22(a) and (b), respectively. For a data high signal, the output does not change state at least untill CMTI $\leq$ 75 KV/μs, while for a data low signal, this event does not occur at least untill CMTI $\leq$ 100 KV/μs. TX emissions are measured for oscillator midband frequency of 500 MHz with RBW of 120 kHz using a quasi-peak detector, and shown in Fig. 23, where frequency spread and peak power reduction due to SSM are clearly observed. Peak power reduction of nearly 10 dB was achieved over the frequency band of interest, due to larger-than-expected mismatches in the SS current sources and hopping oscillator frequency shift, both of which limit the frequency spread. The worst case propagation delay of the TX is less than half the bit period (20 ns) at a data rate of 50 Mb/s. A reverse current of less than 50 nA was measured when a reverse voltage of -5 V was applied, showing that the device indeed exhibits unidirectional operation. The overall measured performance of the TX, including propagation delay and PWD, and comparison with a state-of-the-art LED-based optocoupler [5], is summarized in Table I. At 50-Mb/s data rates, the TX presented in this paper achieves very competitive delay and PWD, with low cycle-to-cycle jitter and better CMTI transient performance.

V. Conclusion

A data-signal-powered OOK TX supporting speeds of up to 50 Mb/s was designed and fabricated in a BiCMOS process. Transient performance of the TX was improved by using fast wakeup and discharge circuits. The TX can withstand a CMTI event of $\leq$75 KV/μs without false turn on/off, which is much better than current state-of-the-art optoisolators. The TX displayed good temperature stability, while radioactive emission levels were reduced by implementing SSM in the oscillator. Since the input electrical behavior of the proposed TX is similar to that of an LED, it can be used as an alternative for the TX in optoisolator-based systems.

References

[1] A. Alessandria, L. La Magna, M. Renna, L. Fragapane, and S. Coffa, “Integrated Si-based opto-couplers: A novel approach to galvanic isolation,” in *Proc. 32nd Eur. Solid-State Device Res. Conf.*, Sep. 2002, pp. 647–650.

[2] P. Mahalingam, D. Guiling, and S. Lee, “Manufacturing challenges and method of fabrication of on-chip capacitive digital isolators,” in *Proc. Int. Symp. Semiconductor Manuf.*, Oct. 2007, pp. 1–4.

[3] R. Kliger, “Integrated transformer-coupled isolation,” *IEEE Instrum. Meas. Mag.*, vol. 6, no. 1, pp. 16–19, Mar. 2003.

[4] S. Kaeriyama, S. Uchida, M. Furumiya, M. Okada, T. Maeda, and M. Mizuno, “A 2.5 kV isolation 35 kV/μs CMR 250 Mbps digital isolator in standard CMOS with a small transformer driving technique,” *IEEE J. Solid-State Circuits*, vol. 47, no. 2, pp. 435–443, Feb. 2012.

[5] *HCPL-7723/0723 50 MBd 2 ns PWD High Speed CMOS Optocoupler*, Avago Technol., San Jose, CA, USA, 2013.

[6] J. Keller, “Design driven LED degradation model for opto-isolators,” in *Proc. 42nd Electron. Compon. Technol. Conf.*, May 1992, pp. 394–398.

[7] S. Baranwal, D. Stout, and A. Premanath, “Emulation of LED input characteristics in BiCMOS process,” U.S. Patent 2015 0326223, Nov. 12, 2015.

[8] M. K. Raja and Y. P. Xu, “A 52 pJ/bit OOK transmitter with adaptable data rate,” in *Proc. IEEE Asian Solid-State Circuits Conf. (A-SSCC)*, Nov. 2008, pp. 341–344.

[9] T. Xia and P. Peng, “A spread-spectrum clock generator with dual-voltage controlled oscillator,” in *Proc. Joint 6th Int. IEEE Northeast Workshop Circuits Syst. TAISA Conf. (NEWCAS-TAISA)*, Jun. 2008, pp. 1–4.

[10] A. Santolaria, J. Balcells, D. Gonzalez, J. Gago, and S. D. Gil, “EMI reduction in switched power converters by means of spread spectrum modulation techniques,” in *Proc. IEEE 35th Annu. Power Electron. Specialists Conf. (PESC)*, vol. 1. Jun. 2004, pp. 292–296.

[11] R. J. Widlar, “New developments in IC voltage regulators,” *IEEE J. Solid-State Circuits*, vol. 6, no. 1, pp. 2–7, Feb. 1971, doi: 10.1109/JSSC.1971.1050151.

[12] I. G. Finvers and I. M. Filanovsky, “Analysis of a source-coupled CMOS multivibrator,” *IEEE Trans. Circuits Syst.*, vol. 35, no. 9, pp. 1182–1185, Sep. 1988.

[13] P. R. Gray and R. G. Meyer, *Analysis and Design of Analog Integrated Circuits*, 2nd ed. New York, NY, USA: Wiley, 1990.

[14] Y.-T. Wang, C. Zhao, R. Geiger, D. Chen, and S.-C. Huang, “Performance verification of start-up circuits in reference generators,” in *Proc. IEEE 55th Int. Midwest Symp. Circuits Syst. (MWSCAS)*, Aug. 2012, pp. 518–521.

[15] K. B. Hardin, J. T. Fessler, and D. R. Bush, “Spread spectrum clock generation for the reduction of radiated emissions,” in *Proc. IEEE Int. Symp. Electromagn. Compat.*, Aug. 1994, pp. 227–231.

[16] Y. Lee and R. Mittra, “Electromagnetic interference mitigation by using a spread-spectrum approach,” *IEEE Trans. Electromagn. Compat.*, vol. 44, no. 2, pp. 380–385, May 2002.

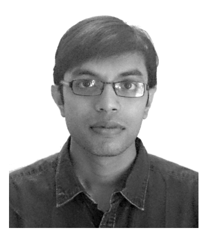

Sreenivasa Mallia S received the B.Tech. degree in electronics and communications engineering from Amrita School of Engineering, Kollam, India, in 2012, and the M.S. degree from the Indian Institute of Technology Madras, Chennai, India, in 2015.

He is presently working as an RF Design Engineer at Qualcomm India Pvt. Ltd., Bangalore, India. His research interests include analog, RF and mixed-signal design.

Sreeram NS was born in a small town close to Bengaluru, India, in 1984. He received the B.E. degree in electronics and communications from JNTU College of Engineering and Technology, Hyderabad, India, in 2006 and the M.E. degree in microelectronics from the Indian Institute of Science (I.I.Sc) Bengaluru, India, in 2008.

In 2006, he joined Texas Instruments, India, as an electrical design engineer and currently leads the isolation design team. His expertise includes designing and architecting low-power, high-speed and EMC-robust isolation products.

Sudhir Komarla Adinarayana was born in Bengaluru, India, in 1982. He received the B.E. degree in electronics and communications from Siddaganga Institute of Technology Tumkur in 2004, and the M.Tech. degree in electronic design and technology from the Indian Institute of Science (I.I.Sc.) Bengaluru in 2006.

He has worked with SiRF Technology and Cypress Semiconductors in analog design in the past. He is working at Texas Instruments since 2010. Present areas of interest are silicon debug, circuit techniques for performance parameters measurement on automated test equipment, and isolation products design and testing.

Sankaran Aniruddhan (S'01–M'07–SM'12) received the B.Tech. degree from the Indian Institute of Technology Madras, Chennai, India, in 2000, and the M.S. and Ph.D. degrees from the University of Washington, Seattle, in 2003 and 2006 respectively.

He interned with the Broadband Communications Group, Texas Instruments, Inc., Dallas, TX, in 2002 and 2003. From 2006 to 2011, he was with the RF-Analog Group, Qualcomm, San Diego, CA, where he worked on cellular transceivers. Since 2011, he has been an Assistant Professor of Electrical Engineering at the Indian Institute of Technology Madras. His current research interests include the design of CMOS RF transceivers and frequency synthesizers.

Dr. Aniruddhan was a recipient of the Analog Devices Outstanding Student Designer Award in 2002.